Journal Name

ARTICLE

Tuning of sunlight-induced self-cleaning and self-healing attributes of an elastomeric nanocomposite by judicious compositional variation of TiO₂-reduced graphene oxide nanohybrid

Suman Thakur and Niranjan Karak*

To achieve combined attributes of shape memory, self-healing and self-cleaning properties within a material is a daunting challenge to the material scientists. Here, hyperbranched polyurethane (HPU)-TiO₂/reduced graphene oxide (TiO₂/RGO) nanocomposite was fabricated to address the afore-stated challenge. The fabricated nanocomposite exhibited composition and dose-dependent mechanical properties with excellent shape recovery ratio (91-95%) as well as shape recovery rate (1-3 min) under exposure sunlight. Most importantly, the nanocomposite demonstrated both repeatable intrinsic self-healing (within 7.5-10 min) and efficient self-cleaning ability by removing a model dirt, methylene blue (within 2-3 h) under the same energy exposure. The study also showed that these novel properties of the nanocomposite can be tuned by judicious choice of amount and composition of the nanohybrid. The presence of a high amount of RGO (0.5-1 weight %) in the nanocomposite helps rapid and efficient healing, whereas a high amount of TiO₂ nanoparticles (5-10 weight %) aids in good self-cleaning property. Therefore, the nanocomposite could be a promising futuristic material for many advanced applications.

Introduction

Smart polymers have carved a distinct niche in materials science over the last few decades.[1,2] Such polymers can response to a stimulus as desired.[3] Shape memory polymer (SMP) is one of the smart polymers which can return from a deformed state (temporary shape) to its original state (permanent shape) upon triggering of a suitable external stimulus.[4] Among the varieties of SMP, polyurethane (PU) is gaining much more interest due to its excellent versatile properties.[5] Even though, all types PU do not demonstrate shape memory effect (SME), most of PU generally exhibit thermo/chemo responsive SME.[6-8] Here it is pertinent to mention that most of hyperbranched polyurethanes (HPUs) exhibit excellent SME which have inherent soft and hard segments.[9] Also, HPU has some unique and desired properties over its linear analog. These include low viscosity, high solubility, good reactivity, easy processing, etc.[10] The design and development of self-healing polymer (SHP) and self-cleaning polymer (SCP) have also attracted significant interest over the past decades as such polymers reduce energy consumption, resources and waste.[11-12] SHP is a class of smart polymers which has the ability to repair the damage caused by

mechanical strain over the time where SCP is a special type of polymer that keeps the surface free from dirt and grime.[13-14] A lot of polymeric materials are developed which exhibit SME, self-healing and self-cleaning properties.[15-22] But it is highly challenging to endow the combined properties in a single material. The structural incompatibility among such types of polymer is one of the crucial reason for this difficulty. In SMP, a permanent network structure is essential to restrict the chain motion and such polymer usually is stiff and possesses high modulus.[5] These structural features of SMP are contradictory to SHP where high chain mobility and interdiffusion are essential.[23] Again, either photocatalytic material or superhydrophobic/superhydrophilic surface is required in SCP for removal of dirt.[14,24] Therefore, it is a fundamental and applied interest to tune these properties in a single polymeric material.

In this context, we found HPU/reduced graphene oxide nanocomposite as an excellent shape memory material.[9] Also, Huang and his co-workers designed a polyurethane/graphene nanocomposite which exhibited repeated healing efficiency by infrared (IR) light, electricity and microwave (MW) energy.[25] Recently, rubber like polymeric material is developed which enable to exhibit both shape memory and healing effect.[26] Again, PU and poly(ε-caprolactone) diol can enable to close the crack above their melting temperature, but the dimension stability of the material is lost in this case.[27] Therefore, thermoplastic HPU which has inherent hard segment is right choice for this purpose and concept of nanohybrid is apparently

Advanced Polymer and Nanomaterial Laboratory, Centre for Polymer Science and Technology, Department of Chemical Sciences, Tezpur University, India-784028, E-mail: karakniranjan@gmail.com (N. Karak); Tel: +91 3712-267327.

a most convenient approach to achieve the both shape memory and healing effects.[28] HPU/sulfur nanoparticle decorated reduced graphene oxide nanocomposite exhibited excellent SME and repeatable healing ability under the exposure of MW and sunlight.[23] To date, we are unaware of any report on polyurethane or its nanocomposite that are featuring SME, self-healing and self-cleaning properties, altogether.

Semiconductor photocatalyst, such as TiO_2 is widely used for photodegradation of organic compounds, especially for decontamination of air and water and hence found to be an exciting material for achieving the photoinduced self-cleaning polymeric materials by using it.[14] The self-cleaning properties of TiO_2 is originated from the photocatalytic oxidative decomposition of organic contaminants.[29] However, high recombination rate of photogenerated electron–hole pairs and only ultraviolet light induced nature of pure TiO_2 are hampered its practical applicability.[30] In this vein, TiO_2/reduced graphene oxide nanohybrid (TiO_2/RGO) exhibited improved photocatalytic activity under visible light or sunlight.[31,32]

Therefore, an attempt has been made to achieve combined attributes of shape memory, self-healing and self-cleaning properties in HPU nanocomposites using different weight% of TiO_2/RGO nanohybrid at variable compositions. Also, the effect of composition and loading of nanohybrid on tuning of self-healing and self-cleaning properties of the nanocomposite were delved into.

Experimental

Materials

Castor oil (Sigma Aldrich, India), 1, 4-butanediol (BD, Merck, Germany) and poly(ε-caprolactone) diol (PCL, M_n= 3000 g mol^{-1}, Solvay Co., UK) were used after drying in an oven. TiO_2 nanoparticles (Sigma Aldrich, India) and 2, 4/2, 6-toluene diisocyanate (TDI, Merck, Germany) were used as received. Xylene (Merck, India) and N, N-dimethylacetamide (Merck, India) were vacuum distilled and kept it in 4A type molecular sieves before use. Other chemicals and solvents were used without further purification. Graphene oxide (GO) was prepared by modified Hummers method. Oxidization of graphite powder was achieved by using a mixture of concentrated sulphuric acid and $KMnO_4$.[33] *Colocasia esculenta* leaf extract was prepared by using conventional method.[33] Monoglyceride of the castor oil was prepared as reported earlier.[10]

Preparation of TiO_2/RGO nanohybrid

Required amount of GO and TiO_2 nanoparticles were taken in water/ethanol (50:50 v/v) system. Then the mixture was stirred for 1 h and sonicated for 10 min to obtain a homogenous dispersion of GO and TiO_2 nanoparticles. Then *C. esculenta* leaf extract (10 mL) was added to the homogenous dispersion (50 mL) present in single necked round bottomed flask and stirred for 5h at room temperature to reduce GO. Three different nanohybrid was prepared using different weight ratio of TiO_2 and RGO (1:1, 5:1 and 10: 1) and they were coded as T_1RGO, T_5RGO and T_{10}RGO respectively.

Preparation of HPU-TiO_2/RGO nanocomposite

An *in-situ* polymerization technique was used to prepare the HPU nanocomposites. Required amounts of PCL (0.002 mol) and BD (0.004 mol) in xylene were taken in a three-necked round bottomed flask which was equipped with a nitrogen gas inlet, a mechanical stirrer and a Teflon septum. Then nanohybrid dispersion in DMAc was added to the mixture. Desired amount of TDI (0.007 mol) was drop wise added in reaction mixture after complete dissolution of PCL in xylene. Then temperature of the reaction was raised to (70±2) °C and continued it for 3h. After achieving the desired viscous mass, 1st step reaction was stop and cooled to room temperature. This was treated as the pre-polymer.

In the 2nd step of the reaction, monoglyceride of castor oil (0.002 mol) as a triol and required amount of TDI (0.002 mol) was slowly added in the prepolymer to maintain overall NCO/OH ratio equal to one. Then the reaction temperature was again raised to (110±2) ºC and stirred continuously for 2.5 h to complete the reaction which was indicated by absence of isocyanate band at 2270 cm^{-1} in FTIR spectrum. HPU was also prepared following same procedure without using TiO_2/RGO nanohybrid for comparing the properties. HPU-TiO_2/RGO nanocomposites were prepared using different weight% of the three nanohybrid separately (T_1RGO, T_5RGO and T_{10}RGO). The nanocomposites were encoded as HPU-T_1RGO1 and HPU-T_{10}RGO10 where last digits implies the nanohybrid content in the nanocomposite.

Instruments and Testing methods

Fourier transform infrared spectra (FT-IR) of the nanohybrid were recorded by a Nicolet (Madison, USA) FTIR impact 410 spectrophotometer over the wave number range of 4000–500 cm^{-1} using KBr pellets. The X-ray diffraction (XRD) patterns of the nanohybrid was carried out at room temperature (ca. 25 °C) by a Rigaku X-ray diffractometer (Miniflex, UK) over a range of 2θ=10-70°. Thermogravimetric analyses (TGA) of the nanohybrid and nanocomposites were done by thermal analyzer, TGA 4000 (Perkin Elmer, USA) with a nitrogen flow rate of 30 mLmin^{-1} at heating rate of 10 ºC min^{-1}. Raman spectra of GO and nanohybrid were taken with SPEX 1403 double monochromator coupled to a SPEX 1442. The samples were excited with an air cooled argon ion laser of wavelength 488 nm. Transmission electron microscope (TEM) analysis was performed with JEOL 2100X electron microscope at operating voltage of 200 kV. The differential scanning calorimetry (DSC) study was done by using DSC 6000, Perkin Elmer, USA at heating rate of 2 ºC min^{-1} under the nitrogen flow rate of 30 mL min^{-1} from -20 to 120 ºC. The tensile strength and elongation at break were measured with the help of Universal Testing Machine (UTM), Jinan WDW 10, Republic of China with a 500 N load cell and crosshead speed 50 mm min^{-1} as well as strain rate of 1 Ns^{-1}. Toughness of HPU and nanocomposites were calculated from the area of stress-strain curve and tensile modulus of nanocomposite was obtained from the slope of linear area in stress-strain curve. Thermocouple (Metravi, 305XL) was used to measure the surface temperature of the sample during self-healing and shape memory tests.

To study the healing performance, the nanocomposite films were cut (10 × 0.2 × 0.015 mm³ in dimension) in transverse direction by a razor blade and sunlight was used to heal the cracked [11 am-2 pm at Tezpur University campus (altitude: 26.63 °N 92.8 °E) in the month of August at sunny days, average temperature (38±1 °C) and humidity (62±1 %)], light intensity: 100,000-110,000 lux]. Healing efficiency was calculated as the ratio of tensile strength of the nanocomposites after healing to the original (before cut). The tensile strengths of the pristine and the healed (repeated up to 3rd cycles) samples were measured by the same UTM. Tensile strengths of HPU and its nanocomposites were measured for at least 4 samples in each case.

The bending shape memory test was done to study the shape memory behaviour under the same stimulus and same condition like self-healing. HPU and its nanocomposite films (40×10×0.4 mm³ in dimension) were taken for this test. Firstly, the polymeric sample was folded in ring form (bending angle 45°) at 60 °C followed by quenching into an ice-salt bath for 10 min at -10 °C. Then the shape recovery of the nanocomposite films was achieved by exposure of direct sunlight in sunny days of month of August. The shape recovery was calculated using the following equation.

$$Shape\ recovery\ (\%) = \frac{(90-\theta)}{90} \times 100 \quad \text{---------------- (1)}$$

$$Shape\ fixity(\%) = \frac{\theta}{90} \times 100 \quad \text{----------------- (2)}$$

Where θ in degree denotes the angle between the tangential line at the midpoint of the sample and the line connecting the midpoint and the end of the curved samples. Shape memory test are performed three times for each sample.

Self-cleaning properties of nanocomposite was evaluated by photocatalytic degradation of methylene blue (MB) as a model compound. In the typical test, nanocomposite film (average weight 0.8-1.0 g) was chopped in to small pieces (dimension almost 5x5 mm²) and this chopped polymer films were immersed in 50 mL of MB solution (60 ppm). Then the solution kept in dark for 1 h to obtain equilibrium. Afterward, the solution was exposed to sunlight (Sunny day, average temperature: 38±1 °C and humidity: 62±1 %, light intensity: 90,000-100,000 lux) for photodegradation of the dye. The concentration change of MB was monitored by measuring UV absorbance intensity at 664 nm at a particular irradiation time intervals.

Result and discussion

Preparation and characterization of nanohybrid

Reduction of GO and formation of nanohybrid were analysed by FTIR spectroscopic technique. FTIR spectra of GO-TiO₂ and T₁₀RGO nanohybrid are shown in Fig. 1(i). After reduction of GO, decreased in broadening of OH stretching band at 3410 cm⁻¹ and disappeared of C=O band 1710 cm⁻¹ indicate that oxygenating group of GO are reduced in the nanohybrid.[33] Also, presence of Ti–O stretching vibration band at 660 cm⁻¹ indicates presence of TiO₂ nanoparticle in the nanohybrid.[34]

Raman spectroscopy is one of the most valuable techniques to analyze the ordered/disordered structures of carbonaceous and titanium oxide-based materials. Fig. 1(ii) shows Raman spectra of GO and T₁₀RGO. Graphene has two well-known characteristic bands D and G bands (~1350 and 1585 cm⁻¹), respectively.[33] These bands are attributed to the local defects/disorders and the sp² graphitic structure, respectively.[34] Fig. 1(ii) shows that the intensity ratio of I_D/I_G increased from 0.82 to 1.09 which can be attributed to more defects/disorders in graphitized structures in nanohybrid.[35] The appearance of the 2D peak in the Raman spectra of GO and nanohybrid at ~2690 cm⁻¹ indicates the presence multilayer graphene sheets in GO and nanohybrid.[35] Also, the peak at 635 cm⁻¹ in the Raman spectra of nanohybrid is assigned to the presence of anatase TiO₂.[36]

XRD patterns of pure TiO₂ nanoparticle and nanohybrid are shown in Fig. 1(iii). The peaks of 2θ values at 25.3, 37.9, 48.0, 54.4, 56.6, and 62.8° are assigned to (101), (004), (200), (105), (211) and (204) planes of anatase TiO₂, respectively.[37] It should be noted that there is no separate peak found for RGO in the nanohybrid. This may be due to the presence of less crystalline RGO than TiO₂. Moreover, the characteristic peak of RGO at around 26° may be masked by main peak of anatase TiO₂ at 25.3°.[38]

TGA thermograms of pure TiO₂ nanoparticles and nanohybrid showed a marginal weight loss in Fig. 1(iv). It is cleared from Fig. 1(iv) that amount of weight loss is increased with increased amount in RGO content in nanohybrid. As RGO contains a few amount of oxygenating group which are degraded at higher temperature. Weight loss of TiO₂ nanoparticle is ascribed to the loss of the adsorbed H₂O and the crystallization of amorphous TiO₂ into anatase TiO₂.[39]

HRTEM image of the nanohybrid demonstrates that the TiO₂ nanoparticles are well-dispersed on the surface of the RGO sheet (Fig. 2a). Fig. 2b shows that the crystal lattice fringes with d-spacing of 0.35 nm corresponding to the (101) plane of the anatase TiO₂.[40] This suggests that the TiO₂ nanoparticles were well-ordered structure and had a high degree of crystallinity.

Mechanical properties of the nanocomposite

The effect of nanohybrid on the mechanical properties of nanocomposite was observed as functions of its loading and composition (Table 1). Generally, hyperbranched polymers demonstrate lower mechanical strength compared to their linear counterparts due to globular and non-entangled structures of former.[41] To overcome this problem, a long chain segment (PCL) was incorporated in the molecular structure of HPU. However, this improvement is also inadequate for many advanced applications due to the presence of monoglyceride of oil which provides plasticizing effect in the HPU matrix. Therefore, the HPU exhibited low tensile strength. Further, HPU exhibited lower tensile modulus compared to its tensile strength due to low stiffness again for the same reason. But after incorporation of nanohybrid, the mechanical properties such as tensile strength, tensile modulus, toughness and elongation at break for all the nanocomposites significantly improved over the pristine HPU (Table 1).
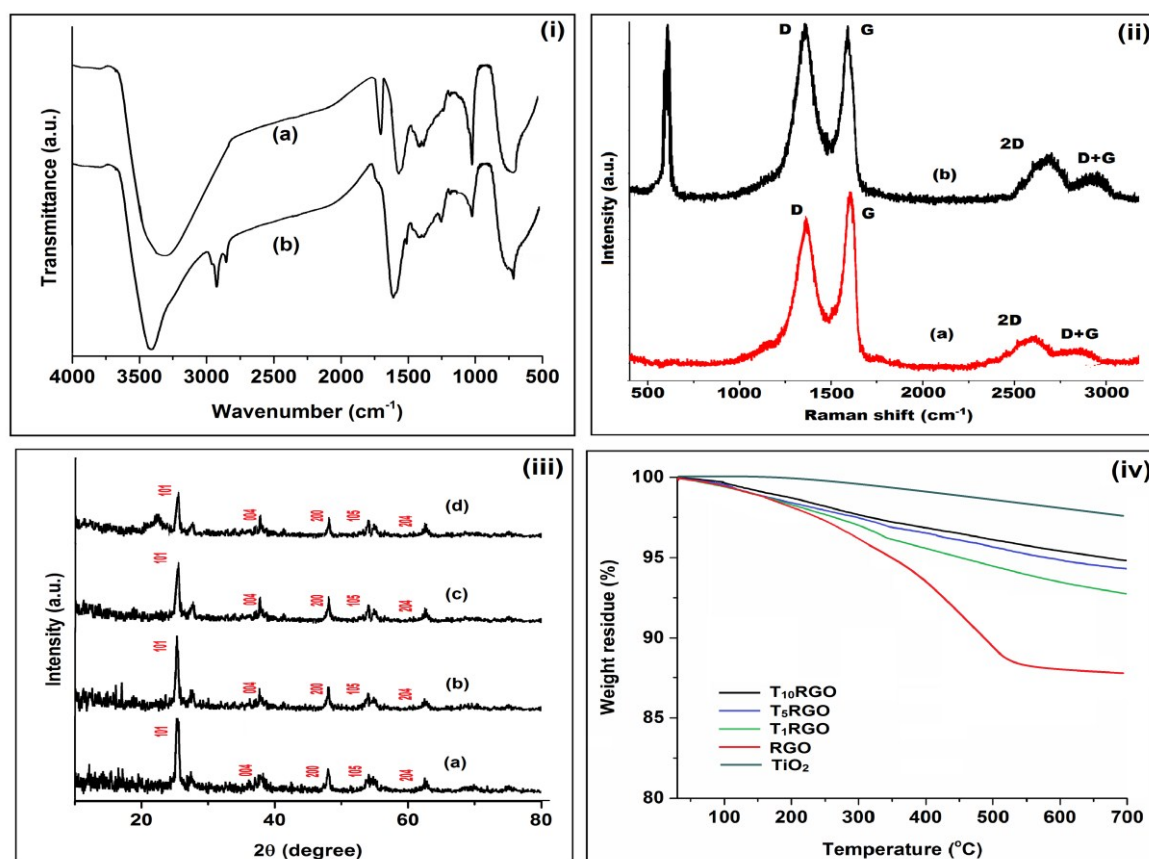
Fig. 1 (i) FTIR spectra of (a) GO-TiO$_2$ and (b) T$_{10}$RGO, (ii) Raman spectra of (a) GO and (b) T$_{10}$RGO, (iii) XRD patterns of (a) TiO$_2$ nanoparticles, (b) T$_{10}$RGO, (c) T$_5$RGO and (d) T$_1$RGO; and (iv) TGA thermograms of TiO$_2$ nanoparticle, RGO and TiO$_2$-RGO nanohybrid.
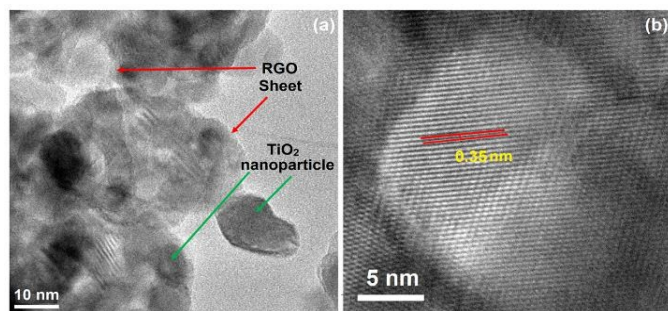
Fig. 2 HRTEM images of T$_1$RGO nanohybrid (a) at low resolution showing the presence of RGO and TiO$_2$ nanoparticle and (b) at high resolution showing crystal lattice fringes of TiO$_2$ nanoparticle.

This is attributed to the good dispersion of nanohybrid, good compatibility and significant interfacial interactions between HPU and nanohybrid.[42,43] The nanohybrid contains sufficient polar hydroxyl groups and polar Ti-O groups. These groups can form covalent and noncovalent bonds with HPU chains as the nanohybrid was incorporated in the 1st step of the polymerization. Thus the hard segments of HPU are stiffen and improved the mechanical properties of HPU nanocomposites.[42] Mechanical properties of the nanocomposites were found to be highly dependent on composition of nanohybrid and its loading.

Table 1 Mechanical properties of pristine HPU and its nanocomposites

Sample	Tensile strength (MPa)a	Tensile modulus (MPa)b	Toughness (MJm-3)c	Elongation at break (%)
HPU	7.2±0.6	3.2±0.4	25.72±2.6	710 ±25
	7.3±0.5[#]	3.5±0.4[#]	26.34±2.9[#]	728 ±21[#]
HPU- RGO 2	27.2 ±0.5	32.2 ±2.4	115.8 ±4.1	1056 ±34
	27.5±0.5[#]	34.6 ±1.8[#]	111.3 ±3.3[#]	950 ±23[#]
HPU- T1RGO 1	23.4 ±0.5	21.4 ±1.8	128.7 ±6.7	1245 ±41
	23.7 ±0.4[#]	21.9 ±1.7[#]	126.2 ±5.8[#]	1221 ±37[#]
HPU- T1RGO 2	25.7 ±0.6	23.7 ±2.1	141.6 ±8.2	1320 ± 35
	25.1 ±0.4[#]	24.2 ±1.7[#]	140.1 ±6.1[#]	1308 ± 28[#]
HPU- T5RGO 1	20.3 ±0.4	18.6 ±1.4	102.1 ±3.4	1043 ± 22
	21.4 ±0.3[#]	19.8 ±1.2[#]	110.8 ±4.5[#]	1108 ± 26[#]
HPU- T5RGO 2	21.8 ±0.2	19.8 ±1.2	110.6 ±4.4	1124 ± 25
HPU- T10RGO 1	17.3 ±0.2	15.9 ±0.9	88.4 ±2.7	910 ± 15
HPU-T10RGO 2	18.2 ±0.3	16.3 ±1.1	95.3 ±3.1	987 ± 26
HPU-T10RGO 5	16.1 ±0.3	14.1 ±1.2	78.4 ±3.3	1035 ± 32
HPU-T10RGO 10	15.3 ±0.4	12.5 ±0.7	69.6 ±2.3	1095± 35

[a] Defined as the stress at the fracture point. [b] Obtained from the slopes of linear areas in stress–strain curves. [c] Calculated by integrating stress–strain curves. [#] Measure at strain rate of 1 Ns^{-1}

COMMUNICATION

Nanocomposite with T_1RGO nanohybrid exhibited superior mechanical properties than nanocomposite with T_5RGO and $T_{10}RGO$ nanohybrids. As RGO has higher aspect ratio than TiO_2 nanoparticle, so mechanical properties are improved in greater extent with the amount of RGO present in the nanohybrid.[33] Also, high amount of nanohybrid deteriorated the mechanical properties may be due to agglomeration of the nanohybrid and irregular load transfer from HPU chains to the nanohybrid. It is most interesting to note that HPU-T_1RGO1 and HPU-$T_{10}RGO5$ contain almost same amount of RGO, but their mechanical properties are drastically different. This may be due to the presence of a high amount of TiO_2 nanoparticles which retard the interaction of RGO with HPU in HPU-$T_{10}RGO10$ nanocomposite. In addition, all the nanocomposites showed higher elongation at break than the pristine HPU. This is due to the presence of RGO in the nanohybrid which is elasto-plastic material.[44]

Thermal properties of nanocomposite

DSC curves of HPU and nanocomposites are shown in Fig. 3. It is seen that the melting temperature of soft segment was considerably dependent on the amount of nanohybrid and the melting temperature shifted to higher temperature with the increased of nanohybrid content. Here, it is important to notice that melting temperature minutely changed with compositional variation of the nanohybrid but highly depended on loading of nanohybrid. As nanohybrid serves as nucleating agent, crystallinity of the nanocomposite enhanced with nanohybrid content.[45] Also, melting temperature of the nanocomposites shifted to a higher temperature due to the presence of more amount of interactions between nanohybrid and HPU chains with increase in amount of TiO_2/RGO nanohybrid in the nanocomposite.

The thermal stabilities of HPU and its nanocomposites were studied using TGA, as shown in Fig. 4. All the thermograms demonstrated two steps degradation profiles for the presence of soft and hard segments in HPU. These suggest that the nature and loading of nanohybrid does not significantly influence the degradation mechanism of the nanocomposite. The initial degradation temperature of the nanocomposite shifted to a notably higher temperature with nanohybrid content. Barrier properties of the nanohybrid are mainly responsible for improving the thermal stabilization of the nanocomposite. Also, the presence of an inorganic component provides additional heat insulting capacity, which stabilizes the nanocomposite against thermal decomposition. Moreover, the presence of strong covalent and non-covalent interactions between nanohybrid and HPU matrix enhances the thermal stability of nanocomposites.

Shape memory behaviors of nanocomposite

Sunlight induced SME was measured for HPU as well as its nanocomposites. Shape recovery and shape fixity values are tabulated in Table 2. All the nanocomposite exhibited excellent SME (Fig. 5). The nanocomposite showed rapid shape recovery than pristine HPU due to presence of nanohybrid that has high sunlight absorbing capacity, especially RGO.[46]
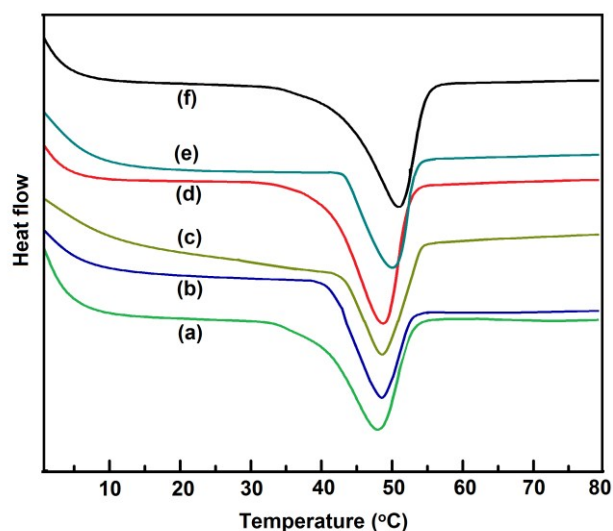
Fig. 3 DSC curves of (a) HPU, (b) HPU-T_1RGO1, (c) HPU-T_5RGO1, (d) HPU-$T_{10}RGO1$, (e) HPU-$T_{10}RGO5$ and (f) HPU-$T_{10}RGO10$.
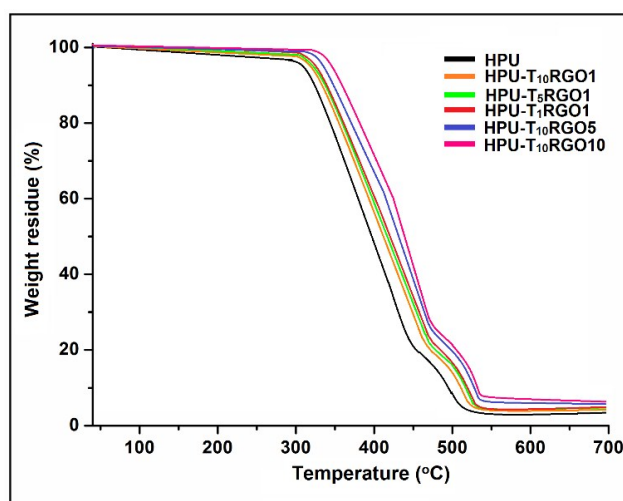
Fig. 4 TGA thermograms of HPU and its nanocomposites.

The effect of composition and loading of nanohybrid on shape memory behavior was also investigated. In particular, the shape recovery time decreased significantly when the amount of RGO is high in the nanohybrid, so T_1RGO based nanocomposite exhibited the highest SME. The rapid shape recovery rate of T_1RGO-incorporated nanocomposite is attributed to the sunlight absorbing ability of the nanohybrid. Here, sunlight was used as the energy source. Shape recovery is achieved by physical changes unlike the other light induced shape memory effect where some chemical reactions are generally taken place such as photo-crosslinking, photo-cleaving reaction, etc.

As, RGO is conducting material, it absorbs the energy from the sunlight and efficiently transfers the absorbed energy to the HPU matrix. Therefore, the nanocomposite reaches its transition temperature easily for recover its shape. The surface temperature was measured and it was found 38.1-38.4 °C at the time of shape recovery which is much lower than T_m of soft segment of matrix.
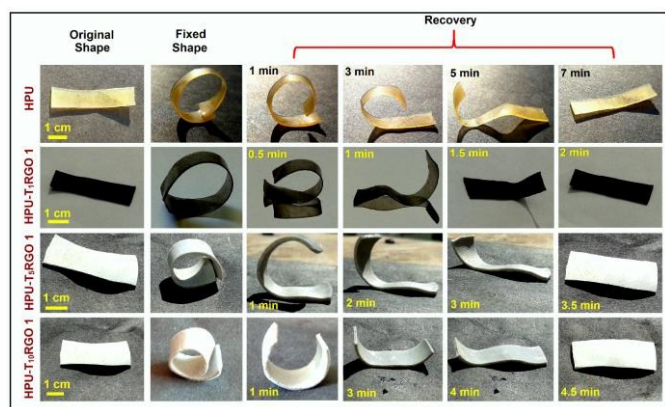
Fig. 5 Series of digital photograph showing shape memory behavior of HPU and its nanocomposites under exposure of sunlight.

Self-healing properties of nanocomposite

Crack of the nanocomposite is effectively healed by the exposure of sunlight as shown in Fig. 6. Healing efficiency of the nanocomposite strongly depends on loading and nature of nanohybrid. Here, it is pertinent to mention that pristine HPU as well as nanocomposites with T_5RGO and $T_{10}RGO$ nanohybrid did not show any healing effect upon exposure of sunlight even for a long time. HPU/ T_1RGO nanocomposites with different loadings were only effectively healed within 7.5-10 min under direct sunlight (Fig. 6a).

It is well-known that SME assist the healing process by bringing the polymeric chains in proximity of the crack.[47] PCL can exhibit the healing effect upon heating above its Tm, but the presence of a hard segment in the polymeric structure is also required as it helps to retain the sample dimension.[26] Again, PU thermoplastic as well as thermoplastic elastomer require higher energy and longer exposure time to recover their shapes compared to their corresponding nanocomposites.[9] Indeed, pristine HPU and all the nanocomposites exhibited SME though only HPU/T_1RGO nanocomposites showed self-healing ability. Both SMP and SHP require rearrangement of polymeric chains but a huge amount of energy is required to soften and interdiffuse the soft segment chains of HPU in the fracture place to heal it. The surface temperature of the sample was found in the range of 44.5 to 45.8 °C at the time of healing. Whereas, comparatively less energy is needed to rearrange the orientation of polymeric chains to achieve the original shape in SMP.[23] This tunable healing property mainly comes from proper variation of the composition of the nanohybrid. From the result, it is cleared that a high amount of RGO is responsible for self-healing as it is a good sunlight absorber.[23] Therefore, HPU/T_1RGO nanocomposite exhibited good healing capability even at low dose level (1 weight%). HPU/T_5RGO and HPU/$T_{10}RGO$ nanocomposites containing 1 or 2 weight% of the nanohybrid did not exhibit healing effect.

This may be due to the presence of a low amount of RGO in the nanocomposites and also the surface of RGO is covered by TiO_2 nanoparticle in the T_5RGO and $T_{10}RGO$ nanohybrids. Therefore, it is enabled to absorb sufficient energy for polymeric chains diffusion. Although, HPU/$T_{10}RGO10$ nanocomposite contains a sufficient amount of RGO in the system (same amount of RGO

present as HPU/T_1RGO1 nanocomposite which showed good healing efficiency), but this nanocomposite did not demonstrate any healing ability. This may be due to the presence of agglomeration of the nanohybrid. As a result, the nanohybrid is not uniformly distributed in the nanocomposite which prevent the efficient transfer of energy to the soft segment of HPU. Also, $T_{10}RGO$ nanohybrid contains high amount of TiO_2 nanoparticles which covered the effective surface area of RGO. Therefore, the nanohybrid also absorbs less amount of sunlight. During the healing process, T_1RGO absorbed energy from sunlight and then transferred the energy to the soft segment of the HPU matrix. This transferred energy aids to soften the segment and the segment starts molecular diffusion towards the crack to repair it. Meanwhile, the hard segment of HPU helps to retain its dimension. Proper variation of composition of the nanohybrid plays a vital role to achieve the desired self-healing ability.

Similar to our earlier work, HPU/T_1RGO nanocomposite also showed repeated healing as it is achieved by the interdiffusion of soft segments of HPU.[23] Thus, even after forth cycle of experiment, the healing ability of the nanocomposite remains almost same (Fig. 6b). Representative stress-strain curves for before and after healing with different repeating cycles are shown in Fig. 6d.

Sunlight induced self-cleaning properties of nanocomposite

In this study, MB was chosen as a model dirt for testing sunlight induce self-cleaning properties of the prepared nanocomposites. Photocatalytic degradation of the dye was investigated by chopped pieces of the nanocomposite film under exposure of sunlight. The degradation of aqueous MB solution based on its concentration changes with time is shown in Fig. 7. Pure TiO_2 nanoparticles can degrade the dye but it efficiency is very poor due to high recombination rate of generated hole/electron (h^+/e^-) pairs. Furthermore, it is only applicable under exposure of UV light which hinders the practical applicability. Therefore, nanohybrid is used to address the above shortcomings. It is well-known that TiO_2/RGO nanohybrid showed enhanced photocatalytic activity over pure TiO_2 nanoparticles and only small amount of RGO (up to 10-20 weight% with respect to TiO_2 nanoparticle) is effective for this enhancement.[48]

Table 2 Shape memory behavior of HPU and its nanocomposites

Sample	Shape recovery ratio (%)	Shape recovery time (min)	Shape fixity (%)
HPU	95.3	7.01	93.6
HPU- RGO 2	98.9	1.58	91.6
HPU- T_1RGO 1	97.8	2.03	92.5
HPU- T_1RGO 2	98.4	1.48	92.1
HPU- T_5RGO 1	96.8	3.44	94.3
HPU- T_5RGO 2	97.2	3.03	92.8
HPU- $T_{10}RGO$ 1	96.2	4.52	94.1
HPU- $T_{10}RGO$ 2	96.6	4.06	94.2
HPU- $T_{10}RGO$ 5	97.3	5.0.3	93.2
HPU- $T_{10}RGO$ 10	94.3	5.56	95.3
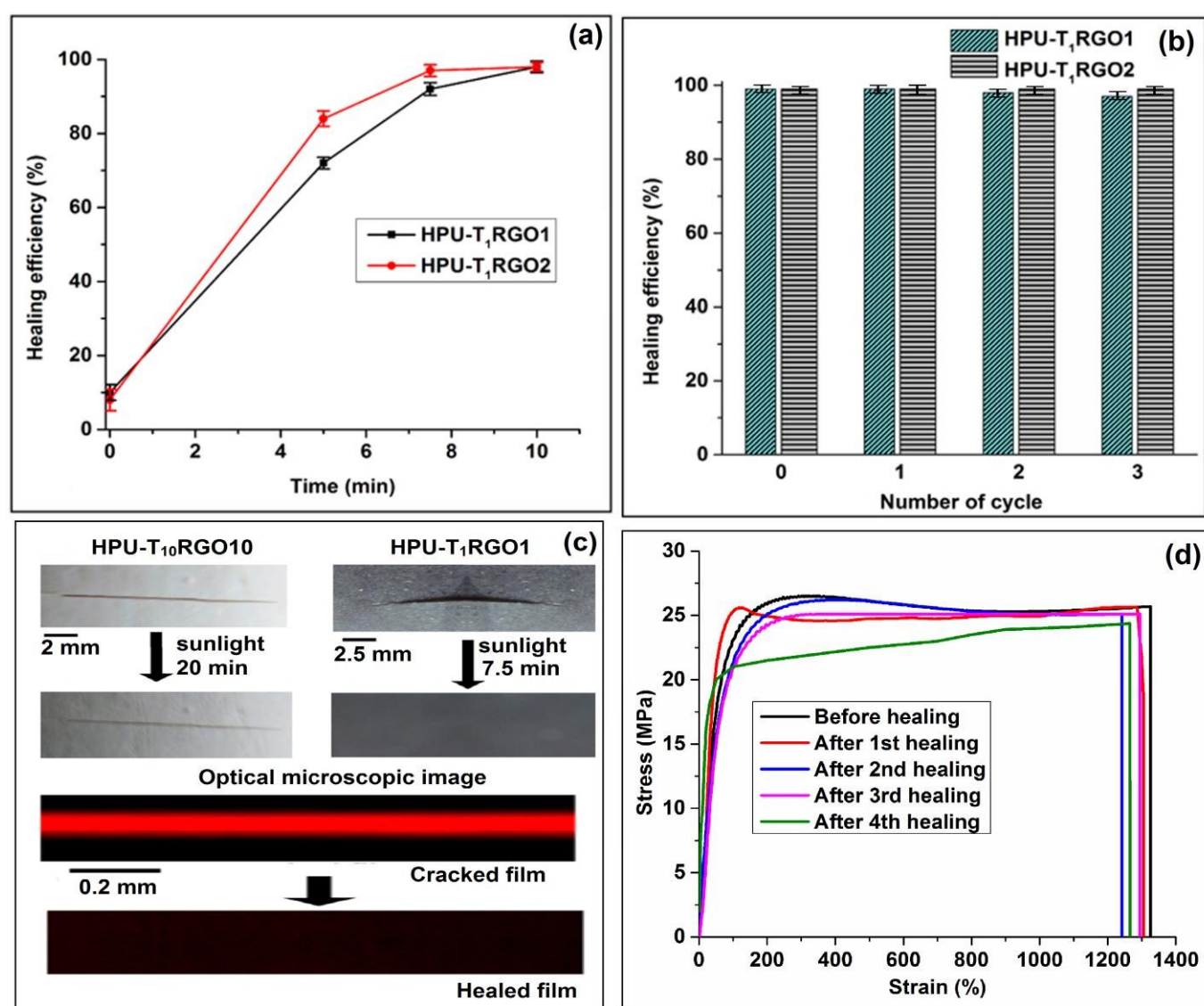
Fig. 6 (a) healing efficiency of the nanocomposites under sunlight, (b) repeatable healing efficiency of the nanocomposites, (c) digital and optical microscopic photographs of cracked and healed nanocomposite films and (d) representative stress-strain profiles of HPU-T$_1$RGO2, before and after healing with different repeating cycles.

Hence, sunlight induced photocatalytic degradation of MB solution led to a significant reduction in MB concentration when HPU/T$_5$RGO and HPU/T$_{10}$RGO nanocomposites were taken as photocatalysts. Whereas, pristine HPU and HPU/T$_1$RGO nanocomposite did not show significant degradation efficiency. As TiO$_2$ nanoparticles are only responsible for degradation of the dye so presence of a high amount of TiO$_2$ nanoparticles in the nanocomposite enhanced the dye degradation rate. Therefore, pristine HPU and HPU/T$_1$RGO nanocomposite were not enabled to show effective dye degradation. During degradation, RGO absorbs energy of sunlight and emits shorter wavelength of light. The emitted energy excites the TiO$_2$ nanoparticles to generate h$^+$/e$^-$ pairs which react with water and O$_2$ to form reactive oxygen species (ROS) such as $\cdot$OH and $\cdot$O$_2^-$. These ROS actually degrade the dye molecules.[49] A blank test without HPU or its nanocomposite was also performed and

extremely slow degradation (only 10%) of the MB was found after 180 minutes of direct sunlight irradiation. The photocatalytic activity of the reused nanocomposite film was checked up to the third cycle as shown in Fig. 7d.

Therefore, to achieve the sunlight induced self-cleaning HPU nanocomposite proper loading and compositional variation of nanohybrid are crucial. The nanocomposite demonstrated significant dye degradability in presence of sunlight. HPU/T$_{10}$RGO10 nanocomposite efficiently degraded the MB dye with 90 min of sunlight exposure with good reusability. Therefore, it can be used as surface coatings material where it can remove the presence of organic dirt and provides a clean surface.
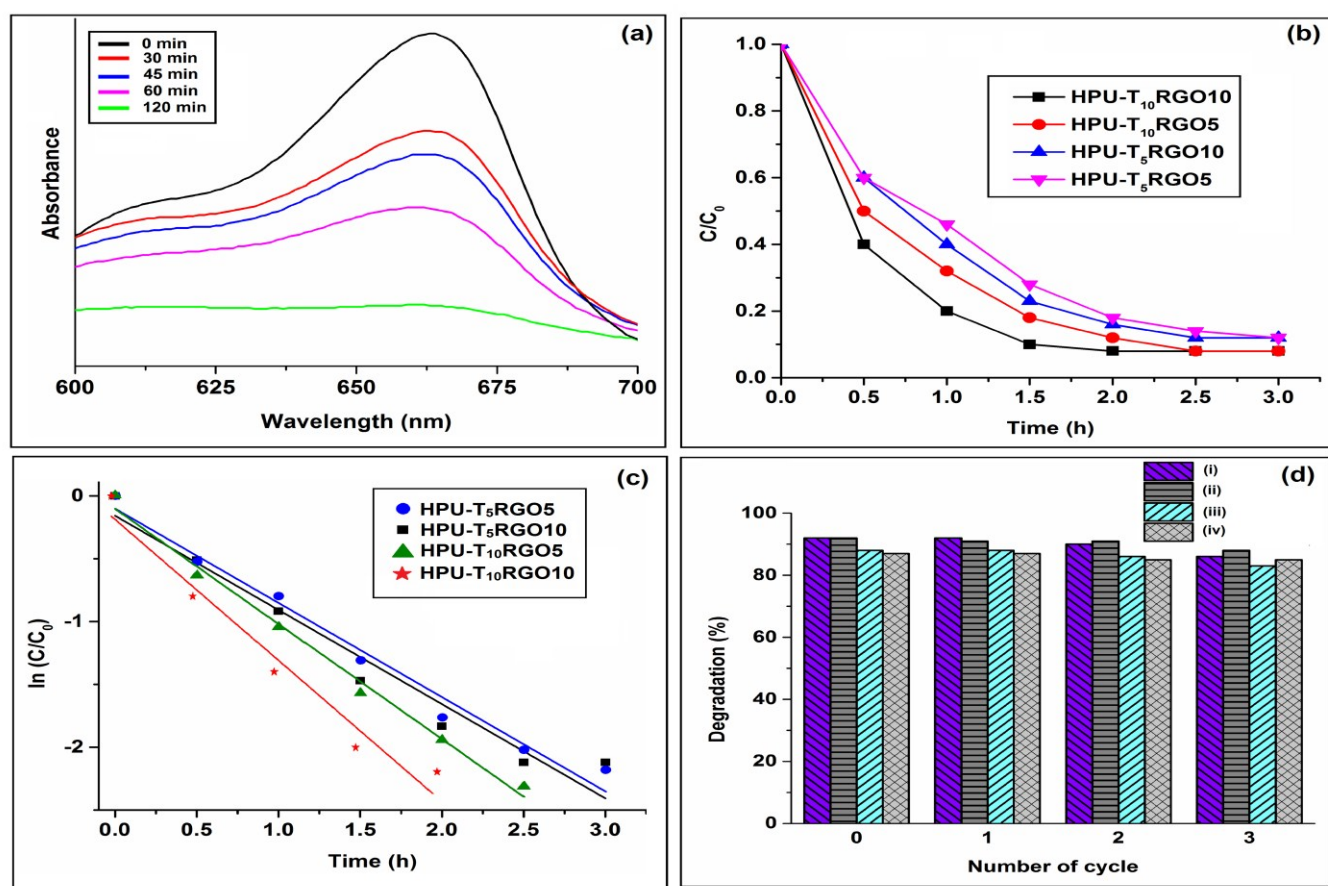
Fig. 7 (a) Time-dependent UV absorption spectra of MB solutions during sunlight irradiation, (b) degradation curves of the MB aqueous solutions by nanocomposite, (c) fitting degradation kinetic curve for pseudo-first order model and (d) photocatalytic efficiency of (i) HPU-T_{10}RGO10, (ii) HPU-T_{10}RGO5, (iii) HPU-T_5RGO10 and (iv) HPU-T_5RGO5 to MB of separate 4 cycles of the continuous dark-adsorption and photocatalytic processes.

Conclusions

We have fabricated tough elastomeric nanocomposites of HPU and TiO$_2$/RGO nanohybrid at different loadings and compositions. All the nanocomposites exhibited excellent thermal and mechanical properties such as tensile strength, tensile modulus, elongation at break and toughness. Interestingly, the fabricated nanocomposites demonstrated SME, self-healing and self-cleaning ability at judicious choice of composition and loading of TiO$_2$/RGO nanohybrid. The simultaneous demonstrating of such attractive properties by a single material may widen the possible applications of the fabricated material in diverse advanced fields.

Acknowledgements

Notes and references

1   F. Liu and M. W. Urban, *Prog. Polym. Sci.*, 2009, **35**, 3–23.
2   D. Roy, J. N. Cambre and B. S. Sumerlin, *Prog. Polym. Sci.* 2010, **35**, 278–301.
3   F. D. Jochum and P. Theato, *Chem. Soc. Rev.* 2013, **42**, 7468-7483.
4   A. Lendlein and S. Kelch, *Angew. Chem. Int. Ed.* 2002, **41**, 2034–2057.
5   S. Thakur and N. Karak, *RSC Adv.* 2013, **3**, 9476-9482.
6   W. M. Huang, B. Yang, Y. Zhao and Z. Ding, *J. Mater. Chem.*, 2010, **20**, 3367-3381.
7   L. Sun, W. M. Huang, H. Lu, K. J. Lim, Y. Zhou, T. X. Wang and X. Y. Gao, *Macromol. Chem. Phys.* 2014, **215**, 2430–2436.
8   W. M. Huang, Y. Zhao, C. C. Wang, Z. Ding, H. Purnawali, C. Tang and J. L. Zhang, *J. Polym. Res.* 2012, **19**, 9952.
9   S. Thakur and N. Karak, *J. Mater. Chem. A*, 2014, **2**, 14867-14875.
10 S. Thakur and N. Karak, *Prog. Org. Coat.* 2013, **76**, 157–164.
11 E. B. Murphy and F. Wudl, *Prog. Polym. Sci.* 2010, **35**, 223–251.
12 S. D. Bergman and F. Wudl, *J. Mater. Chem.* 2008, **18**, 41-62.
13 Y. Yang and M.W. Urban, *Chem. Soc. Rev*. 2013, **42**, 7446-7467.
14 N. M. Bedford and A. J. Steckl, *ACS Appl. Mater. Interfaces* 2010, **2**, 2448–2455.
15 H. Meng and G. Li, *Polymer*, 2013, **54**, 2199-2221.

16   D. Habault, H. Zhang and Y. Zhao, *Chem. Soc. Rev.* 2013, **42**, 7244-7256.

17   R. S. Trask and I. P. Bond, *Smart Mater. Struct.* 2006, **15**, 704–710.

18   S. H. Cho, S. R. White and P. V. Braun, *Adv. Mater.* 2009, **21**, 645–649.

19   K. S. Toohey, N. R. Sottos, J. A. Lewis, J. S. Moore and S. R. White, *Nat. Mater.* 2007, **6**, 581–585.

20   X. Chen, M. Dam, K. Ono, A. Mal, H. Shen, S. R. Nutt, K. Sheran and F. Wudl, *Science* 2002, **295**, 1698–1702.

21   C. M. Chung, Y. S. Roh, S. Y. Cho and J. G. Kim, *Chem. Mater.* 2004, **16**, 3982– 3984.

22   P. A. Charpentier, K. Burgess, L. Wang, R. R. Chowdhury, A. F. Lotus and G. Moula, *Nanotechnology* 2012, **23**, 425606.

23   S. Thakur, S. Barua and N. Karak, *RSC Adv.* 2015, **5**, 2167-2176.

24   P. Chin and D. F. Ollis, *Catal. Today* 2007, **123**, 177–188.

25   L. Huang, N. Yi, Y. Wu, Y. Zhang, Q. Zhang, Y. Huang, Y. Ma and Y. Chen, *Adv. Mater*. 2013, **25**, 2224–2228.

26   C. C Wang, W. M. Huang, Z. Ding, Y. Zhao, H. Purnawali, L. X. Zheng, H. Fan and C. B. He, *Smart Mater. Struct.* 2012, **21**, 115010-8.

27   L. Sun, W. M. Huang, H. Lu, K. J. Lim, Y. Zhou, T. X. Wang and X. Y. Gao, *Macromol. Chem. Phys.* 2014, **215**, 2430-2436.

28   L. Sun, W.M. Huang, Z. Ding, Y. Zhao, C.C. Wang, H. Purnawali and C. Tang, *Mater. Des.* 2012, **33**, 577–640.

29   K. Nakata, M. Sakai, T. Ochiai, T. Murakami, K. Takagi and A. Fujishima, *Langmuir*, 2011, **27**, 3275–3278.

30   G. Tian, Y. Chen, R. Zhai, J. Zhou, W. Zhou, R. Wang, K. Pan, C. Tian and H. Fu, *J. Mater. Chem. A* 2013, **1**, 6961-6968.

31   O. Akhavan, M. Abdolahad, A. Esfandiar and M. Mohatashamifar, *J. Phys. Chem. C* 2010, **114**, 12955–12959.

32   W. S. Wang, D. H. Wang, W. G. Qu, L. Q. Lu and A. W. Xu, *J. Phys. Chem. C* 2012, **116**, 19893-19901.

33   S. Thakur and N. Karak, *Carbon* 2012, **50**, 5331– 5339.

34   D. Graf, F. Molitor, K. Ensslin, C. Stampfer, A. Jungen, C. Hierold and L. Wirtz, *Nano Lett.* 2007, **7**, 238–242.

35   A. C. Ferrari and J. Robertson, *Phys. Rev. B: Condens. Matter*. 2000, **61**, 14095–14107.

36   O. Akhavan, E. Ghaderi and K. Rahimi, *J. Mater. Chem.* 2012, **22**, 23260-23266.

37   M. S. A. Sher Shah, A. R. Park, K. Zhang, J. H. Park and P. J. Yoo, *ACS Appl. Mater. Interfaces* 2012, **4**, 3893–3901.

38   Y. J. Xu, Y. B. Zhuang and X. Z. Fu, *J. Phys. Chem. C* 2010, **114**, 2669-2676.

39   P. Wang, Y. Zhai, D. Wang and S. Dong, *Nanoscale* 2011, **3**, 1640-1645.

40   L. C. Sim, K. H. Leong, S. Ibrahim and P. Saravanan, *J. Mater. Chem. A* 2014, **2**, 5315-5322.

41   S. K. Yadav, S. S. Mahapatra and J. W. Cho, *Polymer*, 2012, **53** (10), 2023-2031.

42   S. Thakur and N. Karak, *ACS Sustainable Chem. Eng*. 2014, **2**, 1195–1202.

43   H. J. Yoo, S. S. Mahapatra and J. W. Cho, *J. Phys. Chem. C* 2014, **118**, 10408–10415.

44   G. Goncalves, P. A. A. P. Marques, A. Barros-Timmons, I. Bdkin, M. K. Singh, N. Emamic and J. J. Gracio, *J. Mater. Chem.* 2010, **20**, 9927– 9934.

45   M. S. Mauter and M. Elimelech, *Environ. Sci. Technol.* 2008, **42**, 5843–5859.

46   S. Thakur and N. Karak, *New J. Chem.*, 2015, **39**, 2146-2154.

47   X. Luo and P. T. Mather, *ACS Macro Lett*. 2013, **2** (2), 152–156.

48   Y. H. Zhang, Z. R. Tang, X. Z. Fu and Y. J. Xu, *ACS Nano* 2010, **4**, 7303-7314.

49   M. Iliut, A. M. Gabudean, C. Leordean, T. Simon, C. M. Teodorescu and S. Astilean, *Chem. Phys. Lett.* 2013, **586**, 127-131.

<u>Graphical Abstract</u>
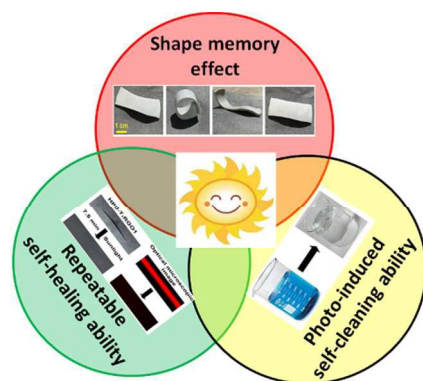
Sunlight induced self-cleaning and healable tough elastomeric hyperbranched polyurethane/TiO₂-reduced graphene oxide nanocomposite is fabricated by an *in-situ* polymerization technique.